OPEN ACCESS
IOP Publishing
Plasma Physics and Controlled Fusion
Plasma Phys. Control. Fusion **61** (2019) 014030 (8pp)
https://doi.org/10.1088/1361-6587/aaeb74

# Impurity transport studies at Wendelstein 7-X by means of x-ray imaging spectrometer measurements*

**A Langenberg[1], F Warmer[1], G Fuchert[1], O Marchuk[2], A Dinklage[1], Th Wegner[1], J A Alonso[3], S Bozhenkov[1], K J Brunner[1], R Burhenn[1], B Buttenschön[1], P Drews[2], B Geiger[1], O Grulke[1,4], M Hirsch[1], U Höfel[1], K P Hollfeld[2], C Killer[1], J Knauer[1], T Krings[2], F Kunkel[1], U Neuner[1], G Offermanns[2], N A Pablant[5], E Pasch[1], K Rahbarnia[1], G Satheeswaran[2], J Schilling[1], B Schweer[2], H Thomsen[1], P Traverso[6], R C Wolf[1] and the W7-X Team[7]**

[1] Max-Planck-Institut für Plasmaphysik, D-17491 Greifswald, Germany
[2] Forschungszentrum Jülich GmbH, Institut für Energie- und Klimaforschung—Plasmaphysik, D-52425 Jülich, Germany
[3] Laboratorio Nacional de Fusión, Asociación EURATOM-CIEMAT, Madrid, Spain
[4] Technical University of Denmark DTU, Dept Phys, PPFE, DK-2800 Lyngby, Denmark
[5] Princeton Plasma Physics Laboratory, Princeton, NJ, United States of America
[6] Auburn University, Auburn, Alabama, United States of America

E-mail: andreas.langenberg@ipp.mpg.de

Received 3 July 2018, revised 5 October 2018
Accepted for publication 25 October 2018
Published 23 November 2018

**Abstract**

This paper reports on the effect of on- and off-axis heating power deposition on the impurity confinement in purely electron cyclotron resonance heated He plasmas on the stellarator Wendelstein 7-X. Therefore, impurity transport times $\tau_I$ have been determined after Fe impurity injections by laser ablations and monitoring the temporal impurity emissivities by the x-ray imaging spectrometer HR-XIS. A significant increase of $\tau_I$ has been observed when changing the power deposition from on- to off-axis heating with energy confinement times $\tau_E$ being mainly unaffected. In addition, the scaling of impurity transport properties with respect to a variation of heating power $P_{\mathrm{ECRH}}$ and electron density $n_e$ has been investigated by keeping the heating power deposition on-axis. The observed $\tau_I$ scaling compares well to known $\tau_I$ scaling laws observed in other machines. A comparison of $\tau_I$ and $\tau_E$ yields an averaged ratio of $\tau_E/\tau_I = 1.3$ and transport times in the range of $\tau_I = 40$–$130$ ms and $\tau_E = 40$–$190$ ms. Comparing those absolute values to neoclassical predictions supports the recently observed nature of anomalous transport in Wendelstein 7-X, given within the up to now investigated operational parameters.

Keywords: impurity transport, impurity confinement, energy confinement, imaging spectrometer, laser blow-off, plasma physics

* Invited paper published as part of the *Proceedings of the 45th Conference on Plasma Physics (EPS)*, Prague, Czech Republic, July, 2018.
[7] R C Wolf *et al* 2017 *Nucl. Fusion* **57** 102020.

Original content from this work may be used under the terms of the Creative Commons Attribution 3.0 licence. Any further distribution of this work must maintain attribution to the author(s) and the title of the work, journal citation and DOI.

## 1. Introduction

Due to non axis-symmetric 3D magnetic fields, impurity transport in the hot plasma core in stellarators is expected to differ from that in tokamaks. In view of reactor-like operation, understanding the impurity transport is a prerequisite for

 © 2018 Max-Planck-Institut fur Plasmaphysik Printed in the UK

steady-state operation, especially for stellarators. These aspects motivate initial impurity transport studies in Wendelstein 7-X (W7-X) at previously—in optimized stellarators-unexplored, reactor-relevant collisionalities. New effects, like potential variations on flux-surfaces [1] or screening effects due to species dependent transport regimes [2] are examples for aspects which attracted recent interest. The ability of W7-X for long pulse operation under fusion relevant plasma conditions offers unique possibilities to study impurity transport even on large transport time scales.

Experimentally, impurity transport investigations have been performed using several techniques, as e.g. monitoring the spatial and/or temporal emissivities of pulsed impurity injections [3–7] or intrinsic impurities [8, 9]. From the experimental data, several transport relevant plasma parameters as the impurity transport time $\tau_I$ [10, 11], the diffusive and convective transport parameters $D$ and $v$ [12–18] or the radial electric field $E_r$ [19], can be determined either directly or from a comparison with transport code calculations.

For an initial, fundamental characterization of transport processes of the recently commissioned W7-X machine [20], this paper presents results of the impurity and energy confinement behavior along the ultimate goal of maximized energy and minimized impurity confinement. As in many large scale fusion experiments, an empirical scaling of the impurity confinement with heating power $P_{\mathrm{ECRH}}$ and electron density $n_e$ has been observed [3, 6], initial systematic $P_{\mathrm{ECRH}} - n_e$ scans have been performed at W7-X in Helium plasmas within two different magnetic configurations comparing measured impurity transport and energy confinement times. Furthermore, the impact of the specific settings of the heating power deposition on the impurity confinement has been investigated.

## 2. Experimental setup

For the investigation of impurity transport properties in W7-X, non recycling Fe impurities have been injected into the plasma using a laser blow-off (LBO) system [11]. After injection, the spatio-temporal evolution of impurities has been monitored using two x-ray imaging spectrometer systems, namely the x-ray imaging crystal spectrometer (XICS) and the high resolution x-ray imaging spectrometer (HR-XIS) [10, 21]. The temporal evolution of the recorded brightness of selected impurity emission lines gives rise to impurity transport times $\tau_I$, being a direct measure of global impurity transport properties [10].

### 2.1. LBO system

The injection of non recycling, mainly metallic impurities such as Al, Ti, Fe, Mo, W, and Si is realized using the LBO technology. Here, atoms, clusters, and macroscopic particles are ablated out of a 2–5 $\mu$m thick material layer covering a glass target by firing a laser onto the target. The laser used at W7-X is a Nd:YAG laser with 1 J laser energy and a maximum repetition rate of 20 Hz. It is guided onto the target holder via several mirrors with the last mirror being steerable allowing to adjust the laser spot position on the target. The glass target holder can mount up to four glass targets and is located 65 cm away from the last closed flux surface of the magnetic standard configuration [22]. An observation camera installed behind the target holder allows an observation of the evaporation process. Depending on the target material, its thickness and the laser spot diameter, impurities in the order of $1 \times 10^{18}$ particles can be evaporated per laser pulse. The detailed design and performance of the system has been described by Wegner *et al* [11].

### 2.2. Imaging spectrometers XICS and HR-XIS

The imaging spectrometers XICS and HR-XIS are equipped with several different crystals for the observation of the x-ray emission of various impurity species in highly ionized charge states. Making use of the imaging properties of a spherical bent crystal, x-rays emitted from the plasma impurities are imaged onto a two dimensional detector area, yielding energy and spatial resolution in horizontal and vertical direction on the detector. A spectral fit [23] and a tomographic inversion [12, 24] of recorded spectra provides radial profiles of the impurity density $n_Z(\rho)$, ion and electron temperature, $T_i(\rho)$ and $T_e(\rho)$, and plasma rotation $v(\rho)$ with $\rho$ defined as the square root of the magnetic flux $\psi$, normalized to the last closed flux surface: $\rho = \sqrt{(\psi/\psi_{\mathrm{LCFS}})}$. For this study, the emission of He-like Fe (FeXXV) has been monitored with a Ge(422) crystal under a Bragg angle of 53.61° using the HR-XIS system. With a viewing geometry from the plasma center towards well above the mid plasma radius ($\rho = 0$–0.6) and a maximal time resolution of $t = 2$ ms, HR-XIS is well suited for transport investigations of impurities located in the bulk plasma. A detailed description of the design and the performance of both spectrometers can be found in [10].

## 3. Global impurity transport at W7-X

This section discusses global transport properties of W7-X based on measurements of impurity transport times $\tau_I$ and energy confinement times $\tau_E$ within a systematic scan of the electron density $n_e$ and the electron cyclotron resonance (ECR) heating power $P_{\mathrm{ECRH}}$. It should be mentioned that the purity of the investigated He plasmas is to some extend reduced, with usual H gas concentrations between 5% and 30% as evident from measurements of the edge He and H densities, possibly affecting the here discussed absolute values of $\tau_I$ and $\tau_E$.

### 3.1. Measurement of impurity transport times

As reported in previous works [10, 11], the measurement of the exponential decay of the impurity signal after a pulsed impurity injection allows to determine the impurity transport time $\tau_I$ that is closely related to impurity transport properties. According to [10], $\tau_I$ is defined as the time constant of the exponential decaying impurity signal after achieving an

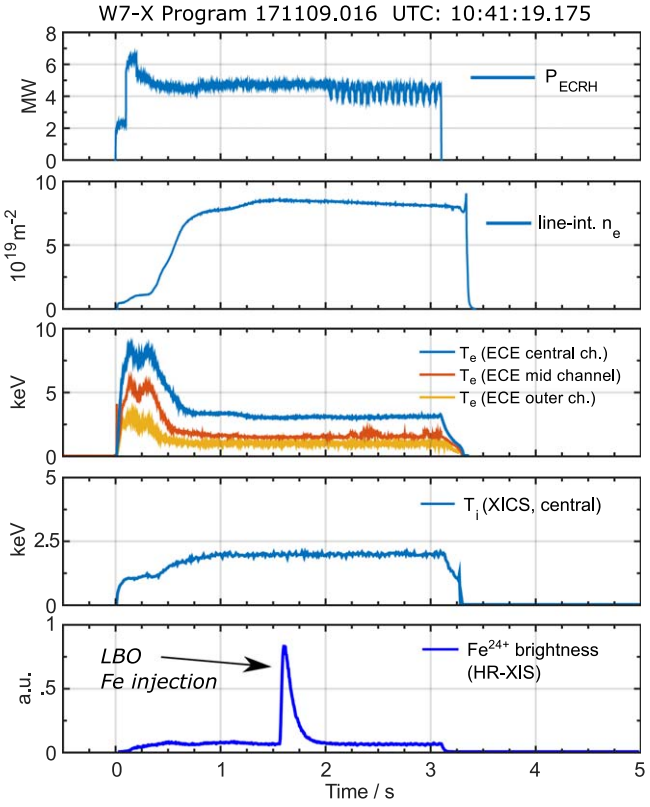


**Figure 1.** Time traces of a centrally ECR heated experimental program in the magnetic standard configuration of W7-X showing the total ECR heating power $P_{\mathrm{ECRH}}$, line of sight integrated density $n_e$, central, mid, and outer radius electron temperatures, central ion temperature, and the brightness of He-like iron emission lines.

ionization equilibrium [10, 11]. Since the impurity signal varies with $T_e$ and $n_e$, we timed the laser pulses for impurity injection within the flat top phase of the experiment with stationary conditions for both $T_e$ and $n_e$.

Figure 1 shows typical time traces of a centrally ECR heated experimental program with a single Fe injection, showing the total heating power $P_{\mathrm{ECRH}}$, the line of sight integrated electron density $n_e$ measured by the interferometer, the central $T_e$ and $T_i$ values as measured by the electron cyclotron emission and XICS diagnostics, and the $Fe^{24+}$ line brightness observed with the HR-XIS spectrometer. The distinct peak in the $Fe^{24+}$ signal at $t = 1.6$ s originates from a single Fe injection via the LBO system, showing the above mentioned exponential decay of the $Fe^{24+}$ signal. The background signal level before and after the Fe injection is induced by the Bremsstrahlung background radiation. The shown time traces demonstrate stationary plasma conditions for $t \geqslant 1.5$ s and also the non perturbing character of the injected Fe tracer impurity.

### 3.2. Impurity transport time scaling

The empirical scaling of $\tau_I$ with respect to $P_{\mathrm{ECRH}}$ and $n_e$ has been investigated in the magnetic standard configuration and the magnetic high mirror configuration of W7-X [22] by performing several experimental programs similar to that shown in figure 1. The label 'high mirror' refers to the higher magnetic mirror term of that configuration compared to the W7-X standard configuration, see also [25]. For the transport analysis, $P_{\mathrm{ECRH}}$ and $n_e$ have been scanned systematically from the lowest possible values up to the maximum available heating power and the appearance of a density limit, terminating the experimental program by a radiation collapse [26]. All programs have been performed with the working gas helium.

The obtained $\tau_I$ values are shown in color code in figure 2 for each experimental program with the corresponding $P_{\mathrm{ECRH}}$ and $n_e$ parameters. In both magnetic configurations, two clear trends can be observed. On the one hand, $\tau_I$ decreases with increasing $P_{\mathrm{ECRH}}$, being well known in literature as power degradation [27–29]. Here, the increased heating power leads to a reduced confinement of impurity species. On the other hand, $\tau_I$ increases with increasing $n_e$. This enhanced confinement of impurities towards higher $n_e$ has also been observed in many other machines.

For a quantitative assessment of these effects, the scaling of $\tau_I$ with $P_{\mathrm{ECRH}}$ and $n_e$ has been fitted to a two dimensional function according to the typical scaling [30]

$$\tau_I \propto \gamma \cdot P_{\mathrm{ECRH}}^{\alpha} \cdot n_e^{\beta} \tag{1}$$

with the free parameters $\alpha$, $\beta$, and $\gamma$. For visualization, the 2D surfaces resulting from the data fit are shown together with the discrete $\tau_I$ values in the top of figure 3 for the standard and high mirror configurations on identical scales, respectively. As already evident from the figure, the scaling of $\tau_I$ with $P_{\mathrm{ECRH}}$ and $n_e$ is very similar for both magnetic configurations. In fact, the determined values for the fit parameters $\gamma$, $\alpha$, and $\beta$ are identical for the standard and the high mirror configuration within the experimental uncertainties as listed in table 1. The bottom of figure 3 compares measured $\tau_I$ values to predicted ones $\tau_I^{\mathrm{REG}}$ according to the scaling law (equation (1)), yielding coefficients of determination (CoD) of 0.66 and 0.75 for the standard and high mirror configurations, respectively.

### 3.3. Energy confinement time scaling

In analogy to the impurity transport time, also the energy confinement time $\tau_E$ is expected to scale according to equation (1) [6]. For the validation of a desired maximized energy and at the same time minimized impurity confinement, $\tau_E$ has been determined for the experimental programs of the $P_{\mathrm{ECRH}} - n_e$ scans discussed in section 3.2 for both magnetic configurations standard and high mirror. The $\tau_E$ values have been evaluated using the diamagnetic plasma energy $W_{\mathrm{dia}}$ as measured by the diamagnetic loop diagnostic [31] and the total heating power $P_{\mathrm{ECRH}}$:

$$\tau_E = W_{\mathrm{dia}} / (P_{\mathrm{ECRH}} - \mathrm{d}W_{\mathrm{dia}}/\mathrm{d}t). \tag{2}$$

To improve statistics, here $\tau_E$ has been evaluated at several time points within the experimental programs, providing more data points for the $P_{\mathrm{ECRH}} - n_e$ scan compared to the impurity transport times evaluated only at times of impurities injected with the LBO.

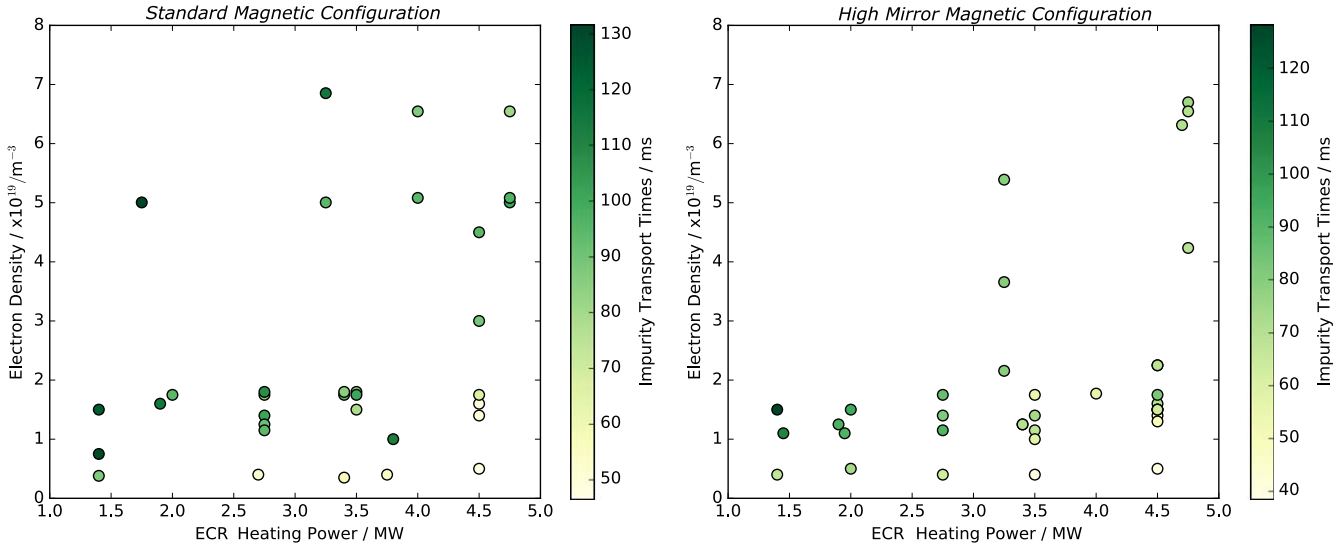


**Figure 2.** Scaling of $\tau_I$ with respect to $P_{\mathrm{ECRH}}$ and $n_e$ in the magnetic configurations standard (left) and high mirror (right).

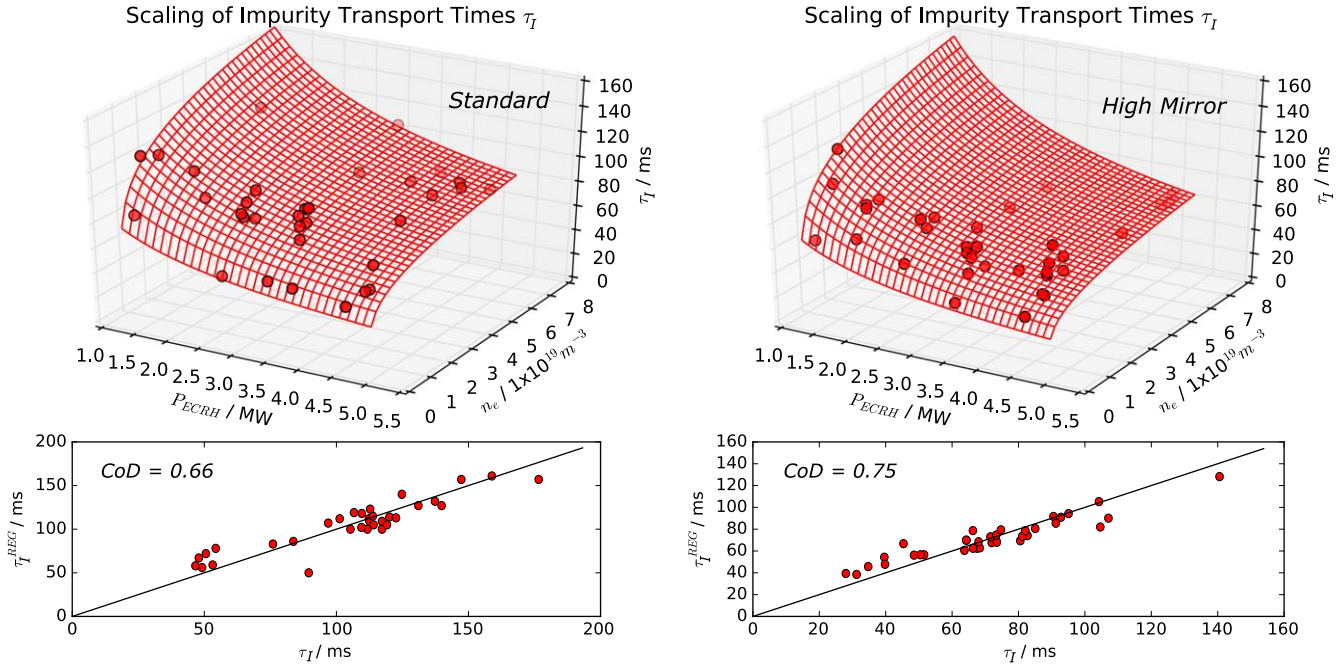


**Figure 3.** Top: fitted $\tau_I$ scaling (meshgrid) from a two dimensional least squares fit of discrete $\tau_I$ values (dots) with respect to $P_{\mathrm{ECRH}}$ and $n_e$ according to equation (1). Bottom: linear regression curve for fitted and actual measured $\tau_I$ values in the magnetic configurations standard (left) and high mirror (right).

The resulting $\tau_E$ values show a pronounced scaling with $P_{\mathrm{ECRH}}$ and $n_e$, very similar to that obtained for $\tau_I$, including the effects of power degradation with increasing $P_{\mathrm{ECRH}}$ and improved confinement with increasing $n_e$ [32]. A quantitative analysis (compare section 3.2) yields the scaling parameters listed in table 2. The $\alpha$, $\beta$, and $\gamma$ values given here compare well to values derived from a more general $\tau_E$ scaling study, including all experimental programs from the last W7-X experimental campaign [32]. Figure 4 compares calculated energy confinement times $\tau_E^{\mathrm{REG}}$ using scaling parameters given in table 2 to actual measured ones, $\tau_E$, with the solid line corresponding to $\tau_E^{\mathrm{REG}} = \tau_E$. For both magnetic configurations, standard and high mirror, the scaling of $\tau_E$ is well described with CoD values of 0.87 and 0.91.

### 3.4. Heating power deposition

Additionally to the $P_{\mathrm{ECRH}}$ and $n_e$ scaling of the impurity transport times, another variation of $\tau_I$ has been observed when varying the ECR heating power deposition from pure on-axis to pure off-axis heating. The different heating deposition profiles have been achieved making use of the ECRH steering launcher, installed at the W7-X ECRH system [33] that allows to deposit the heating power at different radial locations inside the plasma.

**Table 1.** Fitted scaling parameters $\alpha$, $\beta$, and $\gamma$ according to equation (1) for the scaling of $\tau_I$ with $P_{\mathrm{ECRH}}$ and $n_e$ in He plasmas for the magnetic standard and high mirror configurations. Also given is the coefficient of determination, CoD.

| $\tau_I$ scaling parameters | Standard | High mirror |
|---|---|---|
| $\alpha$ | $-0.49 \pm 0.07$ | $-0.60 \pm 0.06$ |
| $\beta$ | $0.19 \pm 0.03$ | $0.21 \pm 0.03$ |
| $\gamma$ | $140 \pm 10$ | $130 \pm 8$ |
| CoD | 0.66 | 0.75 |

**Table 2.** Fitted scaling parameters $\alpha$, $\beta$, and $\gamma$ according to equation (1) for the scaling of $\tau_E$ with $P_{\mathrm{ECRH}}$ and $n_e$ in He plasmas for the magnetic standard and high mirror configurations. Also given is the coefficient of determination, CoD.

| $\tau_E$ scaling parameters | Standard | High mirror |
|---|---|---|
| $\alpha$ | $-0.64 \pm 0.02$ | $-0.60 \pm 0.01$ |
| $\beta$ | $0.23 \pm 0.01$ | $0.25 \pm 0.01$ |
| $\gamma$ | $188 \pm 2$ | $141 \pm 1$ |
| CoD | 0.87 | 0.91 |

For the study of the heating power deposition effect on the impurity confinement, two identical experimental programs, 171 012.018 and 171 012.042 have been performed, guiding the heating power of 4 gyrotrons on radial positions pure on-axis at $\rho = 0$ and off-axis at $\rho = 0.45$ with a total heating power of $P_{\mathrm{ECRH}} = 2.0$ MW.

In both experimental programs, stationary plasma conditions as exemplarily shown in figure 1 have been achieved with static line of sight integrated electron densities as well as static ion and electron temperatures. Figure 5 shows measured $T_i$, $T_e$, and $n_e$ profiles for the on- and off-axis heated programs at the time of the impurity injection around $t = 1.2$ s. While the measured energy confinement times $\tau_E = 90 \pm 2$ ms, the diamagnetic plasma energy contents of $W_{\mathrm{dia}} = 185 \pm 5$ kJ as well as the $T_i$ profiles are nearly identical for both the on- and off-axis heated plasmas, the measured $T_e$ profiles differ significantly from each other, as shown in the top of figure 5. As reported from other stellarators [34] and recently also for W7-X [35], ECR off-axis heating leads to a strong flattening of the $T_e$ profile from the plasma center up to the position of the ECRH deposition, accompanied by a peaking of the $n_e$ profile. While also for this study, the $T_e$ profile flattening is evident from the XICS measurements in well agreement with the Thomson scattering data [36, 37], the $n_e$ profile peaking is not significant within the scattering of profile data given in the bottom of figure 5. However, also here an averaged increase of the $n_e$ profile can be expected as despite the flattened, overall decreased $T_e$ profile, the measured $W_{\mathrm{dia}}$ is very similar for both the on- and off-axis heated plasmas.

Regarding the impurity confinement, a significant change in $\tau_I$ can be observed when changing from on- to off-axis heating. In fact, $\tau_I$ changes from $\tau_I = 86 \pm 1$ ms for on-axis to $\tau_I = 118 \pm 1$ ms for off-axis heating, as shown in figure 6. Here, the left of figure 6 shows time traces of the $Fe^{24+}$ brightness after the Fe impurity injection for on- and off-axis heating. On the right of figure 6, a logarithmic plot of both time traces is shown together with the linear regression curves, yielding the impurity transport times given above.

A more detailed investigation, repeating the shown experimental programs with additional ECRH power deposition profiles as well as analyzing further accessible plasma parameters having impact to the impurity transport, as e.g. the radial electric field $E_r$, is ongoing and will be discussed in forthcoming publications.

## 4. Results and discussion

### 4.1. Impurity and energy confinement

Figure 7 plots the derived scaling parameters $\alpha$, $\beta$, and $\gamma$ of impurity and energy confinement, see tables 1 and 2, for the magnetic configurations standard and high mirror.

Comparing both magnetic configurations, the global impurity confinement turns out to be nearly identical, as demonstrated by the scaling parameters $\alpha$, $\beta$, and $\gamma$ matching each other within the uncertainties, see figure 7, triangles. The same is true for the scaling of the energy confinement with respect to $P_{\mathrm{ECRH}}$ and $n_e$, yielding within the uncertainties nearly equal values for $\alpha$ and $\beta$, see circles in figure 7. However, the absolute $\tau_E$ values are on average slightly enhanced for the magnetic standard configuration, as evident from $\gamma_{\mathrm{Standard}} > \gamma_{\mathrm{HighMirror}}$, see circles in the bottom of figure 7. In fact, the observed improved energy confinement in the magnetic standard configuration is predicted by neoclassical theory as the value of the 'effective helical ripple' $\epsilon_{\mathrm{eff}}$ [38] is much larger in the high mirror ($\epsilon_{\mathrm{eff}} = 2.4\%$) than in the magnetic standard configuration ($\epsilon_{\mathrm{eff}} = 0.7\%$)[39], yielding a larger neoclassical diffusive transport parameter $D_{11}$ in the $1/\nu$ transport regime according to $D_{11}^{1/\nu} \propto \epsilon_{\mathrm{eff}}^{3/2}$ [38] and so a reduced energy confinement for the magnetic high mirror compared to the magnetic standard configuration.

A comparison of the energy and impurity confinement shows a slightly improved energy confinement in both configurations, as reflected by the generally increased scaling parameters: $\{\alpha, \beta, \gamma\}(\tau_E) > \{\alpha, \beta, \gamma\}(\tau_I)$. This enhanced energy confinement over impurity confinement for high $Z$ materials has also been observed for the low confinement regimes at the Tokamaks JET and Tore Supra [6].

Results from neoclassical calculations including measured $T_e$, $T_i$, and $n_e$ profiles [27, 32] shows that neoclassical theory alone can not reproduce the experimental findings without taking into account turbulent transport. In particular, the experimentally obtained $\tau_E$ values are significantly lower than those derived from neoclassical theory, roughly in the order of 50% [32]. A similar trend can be observed also for the impurity transport: while from neoclassical theory, the predicted diffusive transport coefficient profile $D(\rho)$ is constant along $\rho$ with an absolute value of $D < 0.1\ \mathrm{m^2\,s^{-1}}$ [40], the actual measured profile of $D(\rho)$ significantly rises towards the plasma edge with peaking values of $D \leqslant 1.5\ \mathrm{m^2\,s^{-1}}$ as derived from recent Fe impurity transport and earlier Ar

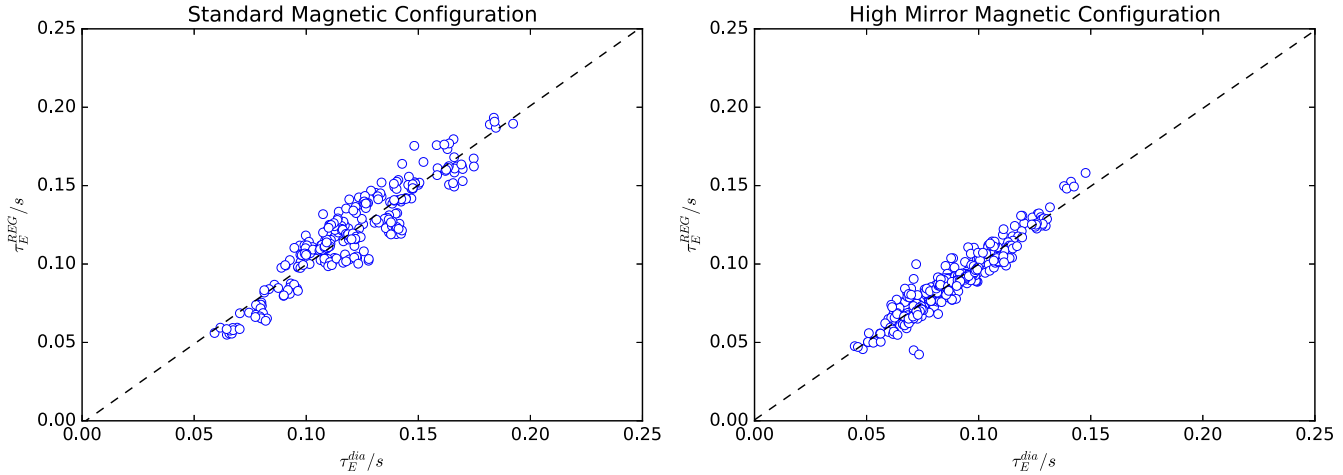


**Figure 4.** Linear regression curve for fitted and actual measured $\tau_E$ values in the magnetic configurations standard (left) and high mirror (right).

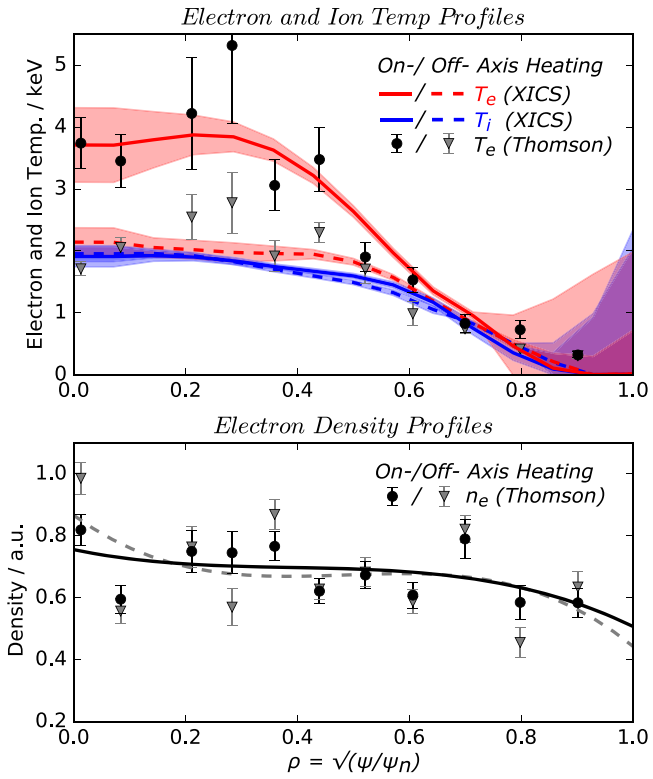


**Figure 5.** Top: ion (blue lines) and electron temperature profiles (red lines) as measured by XICS for on-axis (solid lines) and off-axis (dashed lines) ECRH power deposition together with Thomson scattering data (symbols). The shaded areas as well as the shown error bars correspond to an uncertainty of one standard deviation. Bottom: electron density profiles measured by the Thomson scattering system (symbols) with a spline fit of data points for on-axis (solid line) and off-axis (dashed line) power deposition.

impurity transport studies at W7-X [12, 40]. Both observations suggest significant turbulent contributions to the energy as well as the impurity transport within the machine parameters, W7-X has been operated so far.

### *4.2. Heating power deposition*

In large scale fusion devices, impurities can be prevented from accumulating inside the plasma center by applying a strong central ECR heating. This pretty robust effect is well known and has been observed in several experiments [5, 41]. Hence, the increased $\tau_I$ value for the off-axis ECR heating observed in this study is most probably related to a lack of the impurity pump out by centrally ECRH. As the measured $T_i$ profiles for on- and off-axis heating are identical, the effect might be driven by a profile averaged increase of $n_e$, accompanied by the reduced $T_e$ profile gradients, both effects improving the impurity confinement. Note however, that the additional impact of the strong non neoclassical transport mechanisms observed at W7-X [12, 32, 40] as well as its determining physics quantities is still under investigation and needs further clarification.

## 5. Summary

In this work the impurity and energy confinement scaling of purely ECR heated plasmas has been investigated in two different magnetic configurations of W7-X. The scaling of $\tau_I$ and $\tau_E$ with respect to $P_{\mathrm{ECRH}}$ and $n_e$ both follows a simple power scaling law (equation (1)). On average, the energy confinement is slightly enhanced over the impurity confinement ($\tau_E/\tau_I = 1.3$) with observed absolute values of $\tau_I = 40$–$130$ ms and $\tau_E = 40$–$190$ ms. A comparison of the magnetic standard with the high mirror configuration shows a better energy confinement of the standard configuration, as predicted by neoclassical theory while the impurity confinement is very similar for both configurations. Actually, a more detailed analysis of the here obtained results based on neoclassical theory alone is challenging, as recent results show a significant impact of anomalous transport additionally to the neoclassical transport for both the energy [32] as well as the impurity transport [12, 40]. Here, detailed investigations on the underlying mechanisms are currently ongoing.

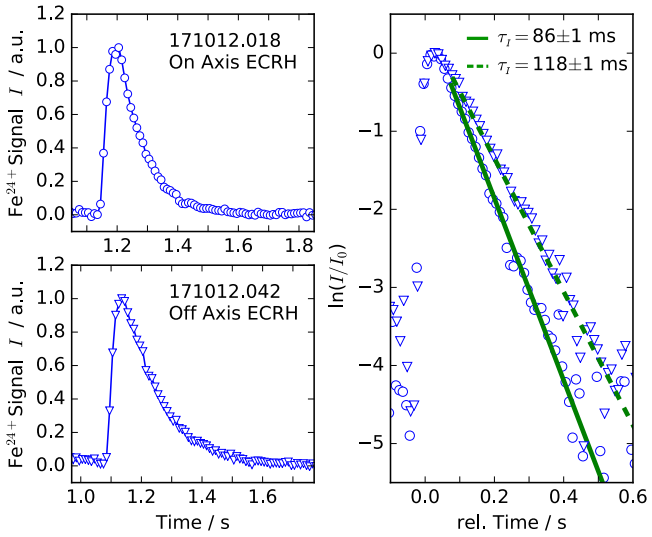


**Figure 6.** Left: time traces of $Fe^{24+}$ line brightnesses after impurity injections for on- and off-axis ECR heating. Right: logarithmic plot of normalized $Fe^{24+}$ time traces and linear fits of $\tau_I$ for on-axis ECRH (solid line) and off-axis ECRH (dashed line).

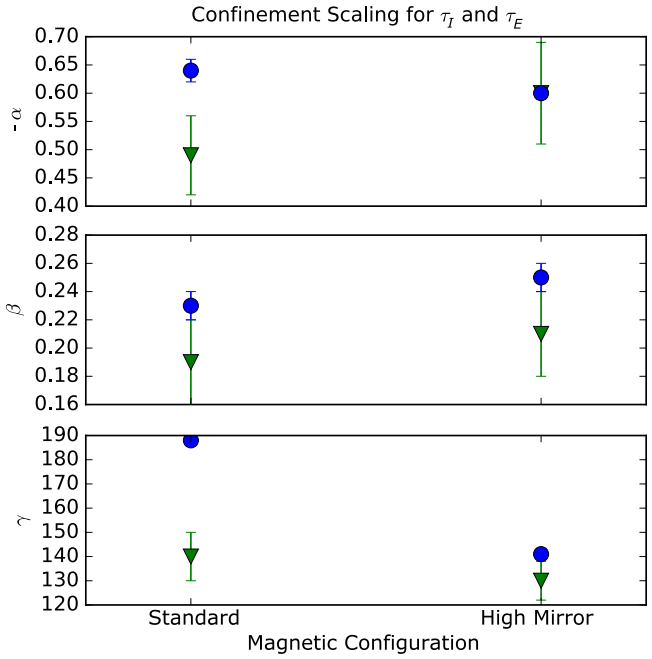


**Figure 7.** Overview on the scaling parameters $\alpha$, $\beta$, and $\gamma$ for the $\tau_I$ (triangles) and $\tau_E$ scaling (circles) in the magnetic standard and high mirror configurations.

A change in the ECR heating power deposition profile induces a significant change in the impurity confinement, most probably related to the well known enhanced impurity pump out induced by central ECR heating [5, 41].

## Acknowledgments

This work has been carried out within the framework of the EUROfusion Consortium and has received funding from the Euratom research and training programme 2014–2018 under grant agreement No 633053. The views and opinions expressed herein do not necessarily reflect those of the European Commission.

## ORCID iDs

A Langenberg https://orcid.org/0000-0002-2107-5488
F Warmer https://orcid.org/0000-0001-9585-5201
O Marchuk https://orcid.org/0000-0001-6272-2605
Th Wegner https://orcid.org/0000-0003-0136-0406
S Bozhenkov https://orcid.org/0000-0003-4289-3532
B Buttenschön https://orcid.org/0000-0002-9830-9641
P Drews https://orcid.org/0000-0002-6567-1601
C Killer https://orcid.org/0000-0001-7747-3066
R C Wolf https://orcid.org/0000-0002-2606-5289

## References

[1] Garcia-Regana J *et al* 2017 *Nucl. Fusion* **57** 056004
[2] Helander P, Newton S L, Mollén A and Smith H M 2017 *Phys. Rev. Lett.* **118** 155002
[3] Scavino E, Bakos J, Weisen H and Team T 2004 *Plasma Phys. Control. Fusion* **46** 857
[4] Nakamura Y *et al* 2003 *Nucl. Fusion* **43** 219
[5] Dux R, Neu R, Peeters A G, Pereverzev G, Mück A, Ryter F, Stober J and Team A U 2003 *Plasma Phys. Control. Fusion* **45** 1815
[6] Mattioli M, Giannella R, Myrnas R, Demichelis C, Denne-Hinnov B, Wit T D D and Magyar G 1995 *Nucl. Fusion* **35** 1115
[7] Marmar E S, Rice J E and Allen S L 1980 *Phys. Rev. Lett.* **45** 2025
[8] Nakamura Y *et al* (The LHD Experiment Group) 2017 *Nucl. Fusion* **57** 056003
[9] Nakamura Y, Kobayashi M, Yoshimura S, Tamura N, Yoshinuma M, Tanaka K, Suzuki C, Peterson B J, Sakamoto R, Morisaki T and The LHD Experiment Group 2014 *Plasma Phys. Control. Fusion* **56** 075014
[10] Langenberg A *et al* 2018 *Rev. Sci. Instrum.* **89** 10G101
[11] Wegner T *et al* 2018 *Rev. Sci. Instrum.* **89** 073505
[12] Langenberg A *et al* (The W7-X Team) 2017 *Nucl. Fusion* **57** 086013
[13] Zhang K *et al* 2016 *Chin. Phys.* B **25** 065202
[14] Arevalo J, Alonso J A, McCarthy K J and Velasco J L 2013 *Nucl. Fusion* **53** 023003
[15] Menmuir S, Carraro L, Alfier A, Bonomo F, Fassina A, Spizzo G and Vianello N 2010 *Plasma Phys. Control. Fusion* **52** 095001
[16] Leigheb M *et al* (The FTU team) 2007 *Plasma Phys. Control. Fusion* **49** 1897
[17] Marchuk O *et al* 2006 *Plasma Phys. Control. Fusion* **48** 1633
[18] Burhenn R *et al* (The W7-AS Team) 2004 *Fusion Sci. Technol.* **46** 115
[19] Pablant N A *et al* (The W7-X Team) 2018 *Phys. Plasmas* **25** 022508
[20] Klinger T *et al* (The W7-X Team) 2017 *Plasma Phys. Control. Fusion* **59** 014018
[21] Pablant N A *et al* 2014 *41st EPS Conf., ECA* vol 38F, p 1.076
[22] Andreeva T 2002 Vacuum magnetic configurations of Wendelstein 7-X *Technical Report* III/270 Max-Planck-Institut für Plasmaphysik, Garching

[23] Langenberg A, Svensson J, Thomsen H, Marchuk O, Pablant N A, Burhenn R and Wolf R C 2016 *Fusion Sci. Technol.* **69** 560
[24] Svensson J and Werner A 2007 *Int. Symp. on Intelligent Signal Processing-WISP* pp 955–60
[25] Geiger J, Beidler C D, Feng Y, Maaberg H, Marushchenko N B and Turkin Y 2015 *Plasma Phys. Control. Fusion* **57** 014004
[26] Fuchert G, Bozhenkov S, Burhenn R, Jakubowski M, Niemann H, Pasch E, Pedersen T S, Zhang D, Wolf R C, Wurden G A and The Wendelstein 7-X Team 2017 *2017 European Conf. on Circuit Theory and Design (ECCTD)* pp 1–4
[27] Dinklage A, Beidler C, Helander P, Fuchert G, Maassberg H, Rahbarnia K, Sunn Pedersen T, Turkin Y and Wolf R C 2018 *Nat. Phys.* **14** 855
[28] van Milligen B P, Carreras B A, Hidalgo C and Cappa A 2018 *Phys. Plasmas* **25** 062503
[29] Yamada H *et al* 2003 *Nucl. Fusion* **43** 749
[30] Burhenn R *et al* 2009 *Nucl. Fusion* **49** 065005
[31] Rahbarnia K *et al* 2018 *Nucl. Fusion* **58** 096010
[32] Fuchert G *et al* (The W7-X Team) 2018 *Nucl. Fusion* **58** 106029
[33] Marsen S, Corre Y, Laqua H, Moncada V, Moseev D, Niemann H, Preynas M, Stange T and The W7-X Team 2017 *Nucl. Fusion* **57** 086014
[34] Stroth U, Geist T, Koponen J P T, Hartfuß H-J, Zeiler P and ECRH, and The W7-AS Team 1999 *Phys. Rev. Lett.* **82** 928
[35] Wolf R *et al* 2018 Electron-cyclotron-resonance heating in Wendelstein 7-X: a versatile heating and current-drive method and a tool for in-depth physics studies *Plasma Phys. Control. Fusion* (https://doi.org/10.1088/1361-6587/aaeab2)
[36] Bozhenkov S *et al* 2017 *J. Instrum.* **12** P10004
[37] Pasch E, Beurskens M N A, Bozhenkov S A, Fuchert G, Knauer J and Wolf R C 2016 *Rev. Sci. Instrum.* **87** 11E729
[38] Helander P *et al* 2012 *Plasma Phys. Control. Fusion* **54** 124009
[39] Grahl M and Geiger J 2018 Web service access on data of vmec equilibrium calculations for W7-X https://svvmec1.ipp-hgw.mpg.de:8080/vmecrest/v1/geiger/
[40] Geiger B *et al* 2018 Observation of anomalous impurity transport in Wendelstein 7-X submitted for publication
[41] Tamura N, Suzuki C, Satake S, Nakamura Y, Nunami M, Funaba H, Tanaka K, Yoshinuma M, Ida K and Sudo S 2017 *Phys. Plasmas* **24** 056118